JOURNAL OF GEOPHYSICAL RESEARCH, VOL. 105, NO. B6, PAGES 13,239–13,252, JUNE 10, 2000

Three-dimensional estimation of elastic thickness under the Louisville Ridge

Suzanne N. Lyons and David T. Sandwell

Scripps Institution of Oceanography, La Jolla, California

Walter H. F. Smith

Laboratory for Satellite Altimetry, NOAA, Silver Spring, Maryland

Abstract. A three-dimensional approach to estimating elastic thickness is presented which uses dense satellite altimetry and sparse ship bathymetry. This technique is applied to the Louisville Ridge system to study the tectonic history of the region. The inversion is performed as both a first-order approximation and a nonlinear relationship between gravity and topography based on *Parker's* [1973] equation. While the higher-order effect on the gravity anomaly is nearly zero for most of the region, the magnitude is significant over the summits of the ridge. Nevertheless, the inclusion of the nonlinear terms has only a minor influence on the elastic thickness estimate within each region, lowering the value by ~1-2 km compared with the linear result. The incorrect assumption of two dimensionality for circular features exhibits a marked effect on the gravitational anomaly, resulting in false sidelobe structure of nearly 20 mGal for large seamounts. Our elastic thickness estimates are compared with the contradictory values obtained in previous studies by *Cazenave and Dominh* [1984] and *Watts et al.* [1988]. We find an increasing elastic thickness along the chain from southeast to northwest, with a discontinuity along the Wishbone scarp. The jump in elastic thickness values northwest of the scarp appears to be an indication of an age discontinuity caused by an extinct spreading center north of the ridge.

1. Introduction

The Hawaiian-Emperor seamount chain serves as the archetype for hotspot volcanism. The Hawaiian chain and its surrounding areas have been the focus of numerous plate flexure studies [e.g., *Vening Meinesz,* 1941; *Moore,* 1970; *Walcott,* 1970; *Watts and Cochran,* 1974; *Suyenaga,* 1979; *Watts,* 1979; *Watts and ten Brink,* 1989; *Wessel,* 1993]. Surprisingly, the Louisville chain (Plate 1), second in size to the Hawaiian group, has not attracted nearly as much attention, probably because of its remote location. The only major bathymetric survey of the Louisville Ridge system was in 1984 [*Lonsdale,* 1986, 1988], and there have been just two attempts at calculating the elastic thickness beneath the different sections of the chain [*Cazenave and Dominh*, 1984; *Watts et al.*, 1988].

Cazenave and Dominh [1984] performed a three-dimensional forward model for geoid height using analog bathymetric maps [*Mammericx et al.*, 1974] and constrained the models with widely spaced Seasat geoid height profiles. However, their study was limited by the relatively low resolution of both the bathymetric maps and the geoid height data. *Watts et al.* [1988] used high-resolution ship bathymetry and gravity anomaly data for their forward model, but they were restricted to modeling along two-dimensional profiles. The two studies yield contradictory values for the elastic thickness under Louisville: Cazenave and Dominh estimate the elastic thickness (T_e) increasing from southeast (12-19 km) to northwest (15-23 km), while Watts et al. estimate T_e increasing from northwest (12.5-17.5 km) to southeast (32.5-42.5 km). Until now there has been no attempt to reconcile these results.

Higher-resolution data from the recent Geosat mission [*McConathy and Kilgus*, 1987] provides precise gravity (3-7 mGal accuracy) over the world's oceans [*Sandwell and Smith*, 1997]. This has been used along with available bathymetric profiles to develop a complete model of inferred bathymetry [*Smith and Sandwell*, 1997]. We introduce a method for determining the elastic thickness which utilizes the complete spatial coverage of the satellite gravity data and sparse ship depth soundings to perform a three-dimensional estimation of elastic thickness. We assess the importance of nonlinear topography to gravity relationships, and we test this method on the Louisville Ridge.

2. Flexure Theory

Dorman and Lewis [1970] investigated the isostatic compensation of continental landmasses by relating the Bouguer anomaly to elevation in the Fourier transform domain. *Parker* [1973] showed that the gravitational anomaly due to an uneven, nonuniform layer could be written as the sum of an infinite series of Fourier transforms:

$$G(\mathbf{k}) = 2\pi\Gamma(\rho_1 - \rho_2)e^{-2\pi|\mathbf{k}|s} \sum_{n=1}^{\infty} \left(\frac{|2\pi\mathbf{k}|^{n-1}}{n!} F\{t^n(\mathbf{r})\} \right), \qquad (1)$$

where s is the average depth of the area, Γ is the gravitational constant, $\mathbf{k}$ is the wavenumber vector ($1/\lambda_x$, $1/\lambda_y$), and $F\{t^n(\mathbf{r})\}$ is

Paper number 2000JB900065.
0148-0227/00/2000JB900065$09.00

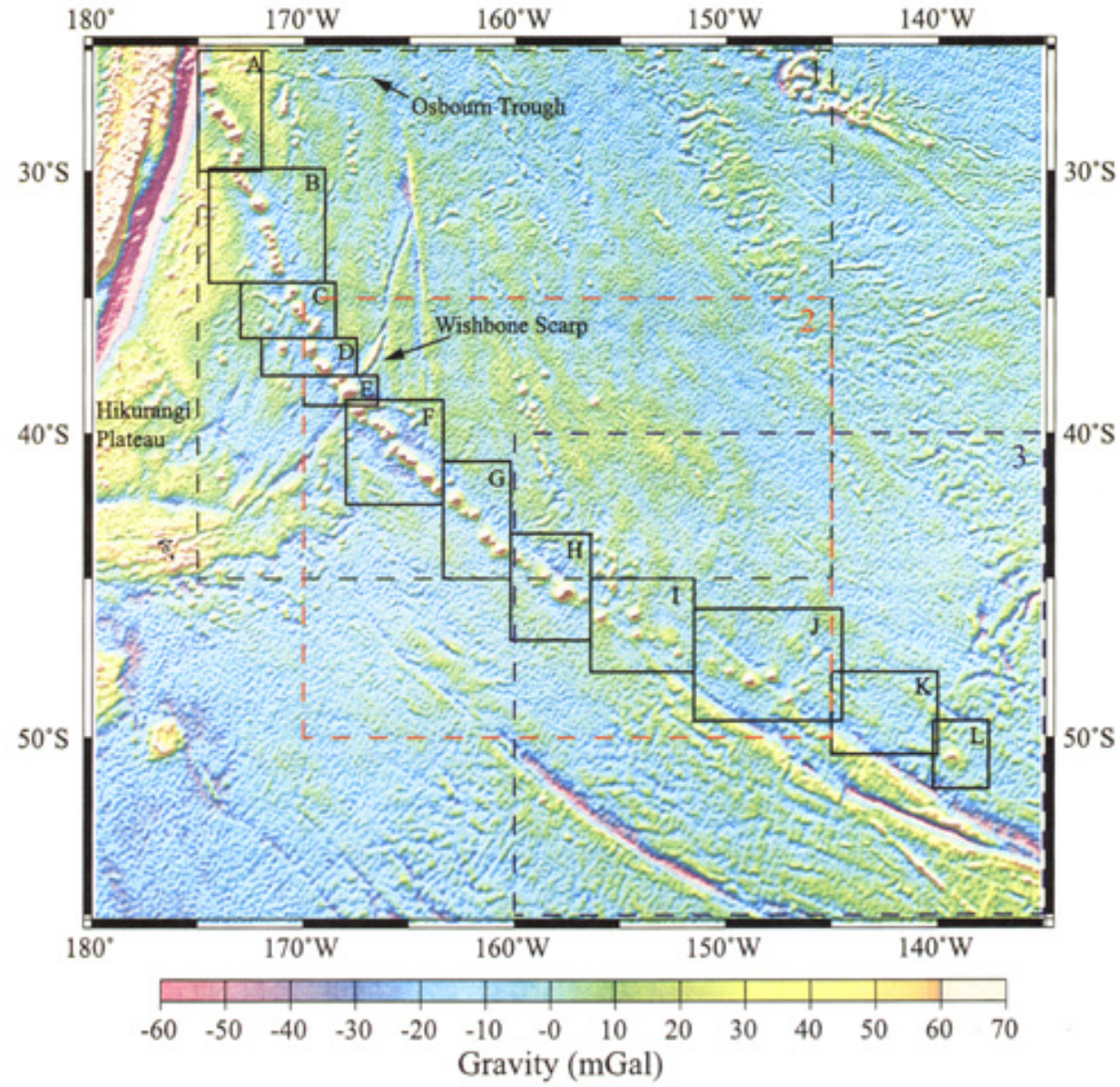

Plate 1. Gravity anomaly over the Louisville Ridge system, southwest Pacific. Gravity data are taken from *Sandwell and Smith* [1997]. Colored dashed boxes (1-3) represent regions over which gravity was inverted to produce bathymetric predictions. Each box is approximately 1000 x 1000 km^2 in order to include the very long wavelengths in the inversion. Smaller black boxes (A-L) represent subregions within which predicted bathymetry was compared to available ship data. The rms values were calculated within each subregion and determined the best fitting parameters for that subregion.

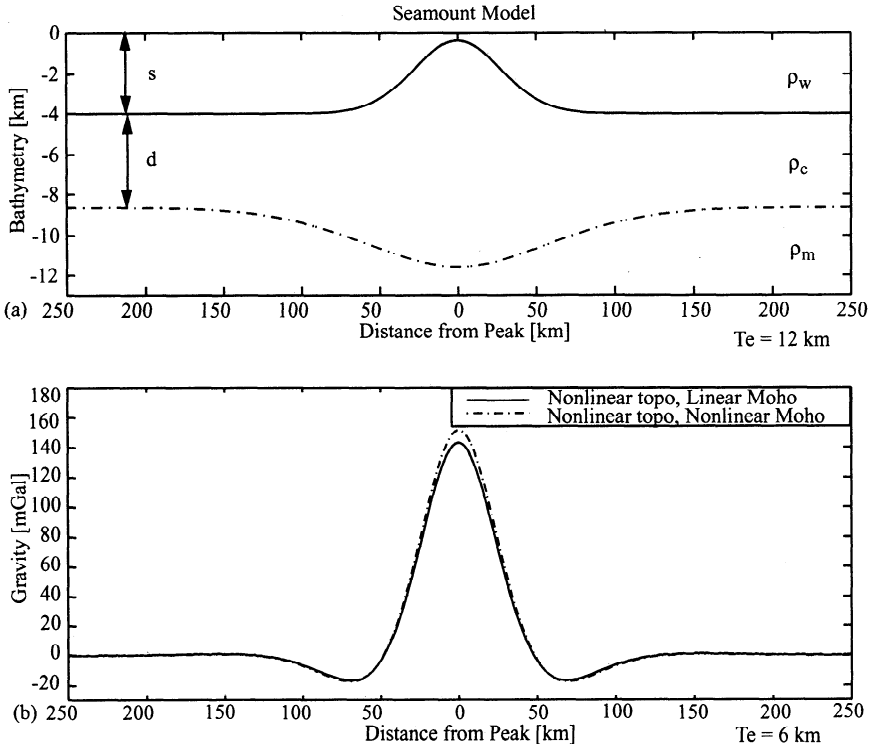

Figure 1. (a) Model of a topographic load on an elastic plate overlying a fluid asthenosphere. The load is a Gaussian seamount of height of 3.6 km, σ=20 km, ρ_c=2800 kg m^{-3}, ρ_m=3400 kg m^{-3}, and T_e=12 km. (b) The nonlinear effects of the Moho for this seamount model, with T_e=6 km. The solid line represents the gravity anomaly determined by equation 2, including the first term, the linear effect of bathymetry and Moho topography, and the first seven terms of the second term, the nonlinear effect of bathymetry. The dashed line also includes the first seven terms of the third term, the nonlinear effect of the Moho topography. The maximum difference between these two signals is 10 mGal (<7%).

the two-dimensional Fourier transform of the nth power of topography of the layer. We use these two approaches, along with the thin elastic plate flexure model (Figure 1a) [e.g., *McKenzie and Bowin*, 1976; *Banks et al.*, 1977; *McNutt*, 1979], to write the gravitational anomaly as the sum of a linear term (first term) and two nonlinear terms, (second term) and (third term):

$$G(\mathbf{k}) = 2\pi\Gamma(\rho_c-\rho_w)e^{-2\pi|\mathbf{k}|s}B(\mathbf{k})\left[1-e^{-2\pi|\mathbf{k}|d}R(|\mathbf{k}|)\right]$$
$$+2\pi\Gamma(\rho_c-\rho_w)e^{-2\pi|\mathbf{k}|s}\sum_{n=2}^{\infty}\left(\frac{|2\pi\mathbf{k}|^{n-1}}{n!}F\{b^n(\mathbf{r})\}\right) \quad (2)$$
$$+2\pi\Gamma(\rho_m-\rho_c)e^{-2\pi|\mathbf{k}|(s+d)}\sum_{n=2}^{\infty}\left(\frac{|2\pi\mathbf{k}|^{n-1}}{n!}F\{m^n(\mathbf{r})\}\right),$$

where the first term on the right-hand side is due to both the bathymetry of the ocean floor, $b(\mathbf{r})$, and the Moho topography, $m(\mathbf{r})$, the second term on the right-hand side is due solely to the bathymetry; and the third term on the right-hand side is due entirely to the Moho. Using the thin elastic plate flexure model, the Moho topography is given by

$$m(\mathbf{r}) = F^{-1}\left\{-\left(\frac{\rho_c-\rho_w}{\rho_m-\rho_c}\right)R(|\mathbf{k}|)B(\mathbf{k})\right\}, \quad (3)$$

with $R(|\mathbf{k}|)$, also known as the flexural response function, given by

$$R(|\mathbf{k}|) = \left(1+\frac{D|2\pi\mathbf{k}|^4}{g(\rho_m-\rho_c)}\right)^{-1}. \quad (4)$$

The flexural rigidity of the plate, D, is defined as $D=(ET_e^3)/[12(1-\nu^2)]$, d is the average crustal thickness (6 km), E is Young's modulus (1x10^{11} N m^{-2}), ν is Poisson's ratio (0.25), T_e is called the elastic thickness of the plate, and ρ_m, ρ_c, and ρ_w are the densities of the mantle (3400 kg m^{-3}), bathymetry (2600-3000 kg m^{-3}), and seawater (1025 kg m^{-3}), respectively.

Our approach for estimating elastic thickness, which uses dense gravity measurements and sparse bathymetric soundings, relies on a linear relationship between gravity and bathymetry so we first assess the nonlinear terms in equation (2). Under the loading conditions of the Louisville ridge we expect that the nonlinear terms due to topography are large and must be accounted for, while the nonlinear terms due to Moho topography are small and can be neglected. To investigate the nonlinear Moho terms (equation (2) third term) for this region, we consider a worst-case scenario of a large seamount (Gaussian height of 3.6 km, σ=20 km, ρ_c=2800 kg m^{-3}) loading a weak elastic plate (T_e of only 6 km); this will result in maximum Moho topography and thus maximum nonlinear contribution. This T_e is close to the smallest distinguishable value of 5 km for our method. The maximum difference between the gravity calculated with just the first-order Moho (solid line in Figure 1b) and the gravity that includes the nonlinear terms (2-7) (dashed line) is ~10 mGal (7%). This difference drops quickly as T_e increases, though, and for a more reasonable plate thickness of 12 km the nonlinear effect is only ~2 mGal (<2%). Thus we are able to justifiably disregard the higher-order effects of the Moho topography. With the nonlinear terms accounted for, equation (2) becomes

$$G(|\mathbf{k}|) = Z(|\mathbf{k}|)B(\mathbf{k}) + N(|\mathbf{k}|,t), \quad (5)$$

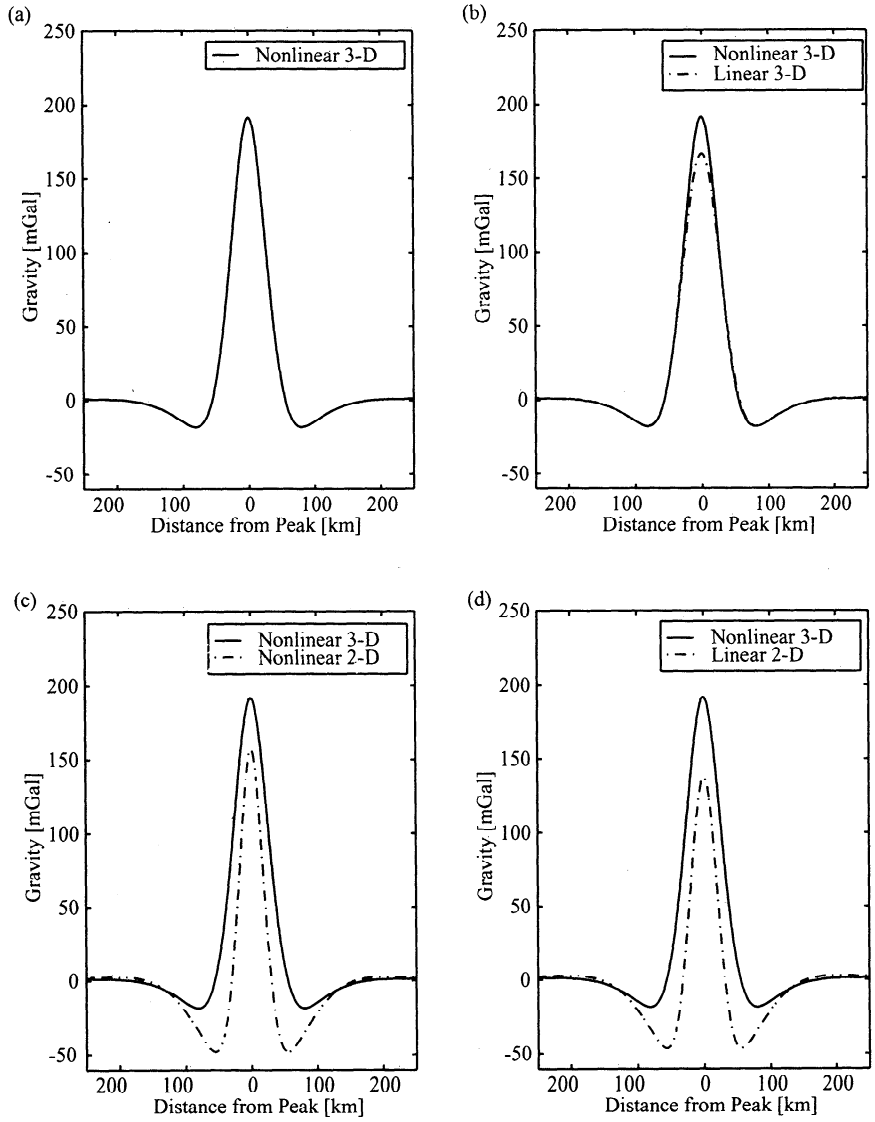

Figure 2. Model illustrating nonlinear and dimensionality effects. Each model represents the gravity anomaly due to a topographic load placed on a flat surface (no flexure). (a) and (b) Modeled by a Gaussian with the same parameters as Figure 2a. (c) and (d) Modeled by a ridge with the same parameters as in Figures 2a and 2b. The solid line represents the true gravity anomaly over the model Gaussian seamount and is shown for comparison. Figure 2b demonstrates the effect of ignoring the nonlinear terms of *Parker's* [1973] equation for a three-dimensional feature. The linear estimate (dashed) has similar flanks to the nonlinear (solid), but shows a much smaller peak amplitude. Figure 2c shows the effects of improper dimensionality assumptions on the gravitational anomaly in the nonlinear case. The flank structure is noticeably changed, reducing each side by 20 mGal and causing a shift in the peak amplitude of ~30 mGal. The most common inversion techniques assume both linearity and two dimensionality, yielding a model (Figure 2d) that has insufficient peak amplitude and a false negative sidelobe, leading to an overestimate in T_e.

where $N(|\mathbf{k}|,t)$ contains the nonlinear contributions from the bathymetry and $Z(|\mathbf{k}|)$ is called the "admittance function" and represents the gravity anomaly in the wavenumber domain resulting from the compensation of a point load.

Owing to the ease of inverting a linear system, most of the previous elastic thickness studies have ignored the nonlinear contributions [*Watts*, 1978; *Dixon et al.*, 1983; *Cazenave and Dominh*, 1984; *Watts et al.*, 1988; etc.]. This is, in general, a good approximation, as the linear contribution is usually 85-90% of the total gravity anomaly [*McNutt*, 1979; *Goodwillie*, 1995]. However, the omission of nonlinear terms in bathymetric/gravitational modeling could be detrimental in areas where the higher-order terms grow large, such as regions where the relief of the topography approaches the mean depth [*Parker*, 1973], areas of short-wavelength, uncompensated topography, or wherever the lithospheric deflection is comparable to the elastic thickness [*Ribe*, 1982]. As this encompasses numerous regions of the world's oceans, some analyses of the gravity/topography relationship over volcanic features have included these terms [*Baudry and Calmant*, 1991; *Goodwillie*, 1995; *Sichoix and Bonneville*, 1996].

Figures 2a and 2b demonstrate the importance of the higher-order bathymetric terms when modeling gravitational anomalies due to a topographic load. To investigate an extreme case (large, short-wavelength feature on a thin plate), we again consider the Gaussian model in Figure 1, but with an elastic thickness of 12

km. The results are shown in Figures 2a and 2b. The solid profile in both plots includes the nonlinear terms (up to N=7), while the dashed profile in Figure 2b is the linear approximation. Note that the inclusion of higher-order terms has very little effect on the flanks of the anomaly but exerts a strong (~13%) influence on the peak amplitude, suggesting that the inclusion of the nonlinear relationship is important when attempting to fit anomaly peaks, especially in regions where the topography nears the ocean surface but that the linear approximation should be satisfactory for fitting on the sides.

Figures 2c and 2d show the effect of correct dimensionality on gravity anomaly models. For the past two decades, flexure modelers have had sufficient spatial coverage in continental data to model the gravity/topography relationship in three dimensions, thus being able to properly account for the dimensionality of the modeled features [e.g., *Lewis and Dorman*, 1970; *Banks et al.*, 1977; *McNutt and Parker*, 1978]. Marine geophysical studies, however, have, until recently, been limited by the availability of ship data along profiles. This has forced most researchers to perform their modeling techniques either by using bathymetric maps in areas of dense ship tracks [*McNutt*, 1979; *Sichoix and Bonneville*, 1996; *Hébert et al.*, 1999; etc.] or by looking at only two dimensions: distance along track and depth [*Watts*, 1978; *Ribe and Watts*, 1982; *Dixon et al.*, 1983; etc.]. For *Parker's* [1973] equation to hold in two dimensions, two assumptions must be made: the length of the feature is much greater than the width (such as a ridge) and the ship track/profile crosses approximately perpendicular to the feature. In general, the length of the feature should be >250-300 km before the bathymetry can be safely assumed as two-dimensional (2-D) [*Ribe*, 1982]. These assumptions severely limit the number of ship tracks that can be used with any degree of confidence within a given area.

In Figure 2c the solid line again represents the nonlinear seamount model but is compared with the gravity over a ridge with the same parameters as the seamount (dashed line). Both models contain the nonlinear effects so the differences between the profiles should be due solely to dimensionality. Here both the peak amplitude and the flank shape for the ridge are different from that of the seamount. The assumption of a 2-D structure for a seamount causes a false negative sidelobe in the gravity anomaly, shifting the peak of the anomaly by a significant amount and creating a gravitational low at the base of the signal.

Figure 2d shows the combined effects of these two most common assumptions in flexural modeling. The solid line once again represents the true gravity signature over a model seamount, while the dashed line represents an approximation of a linear relationship between topography and gravity over a feature modeled as a two-dimensional structure. By using somewhat extreme parameters (large feature on a plate with low T_e), we see that the resultant misfit is almost 20 mGal along the flanks and up to 50 mGal at the peak. Trying to fit this model by altering the elastic thickness parameter would yield a T_e higher than the true one if this feature were actually a seamount rather than a ridge. Therefore, much caution should be taken in areas with high-amplitude, circular features, and, if possible, both the nonlinear effects as well as the correct dimensionality should be included in any gravitational model.

3. Method

For the past few decades, limited data meant that marine geophysicists could only perform flexure studies using gravity and bathymetry along sparse ship tracks. However, with the advent of satellite altimetry to determine the Earth's geoid, it has been possible to investigate the gravity/bathymetry relationship in three dimensions [*Dixon et al.*, 1983; *Kogan et al.*, 1985; *Cazenave and Dominh*, 1984; *Calmant et al.*, 1990]. With the recent declassification of the dense Geosat altimetry data, the quality and resolution of the geoid have increased substantially, making it possible to model in three dimensions with much more reliability (see Figure 3). In our study, we used the *Sandwell and Smith* [1997] 2-min gravity grid, version 9.2, to invert for bathymetry on a grid, the *Smith and Sandwell* [1997] predicted bathymetry, version 6.2, to give us an estimation of the nonlinear anomaly contribution and the available ship bathymetry data along profiles to compare with our predictions.

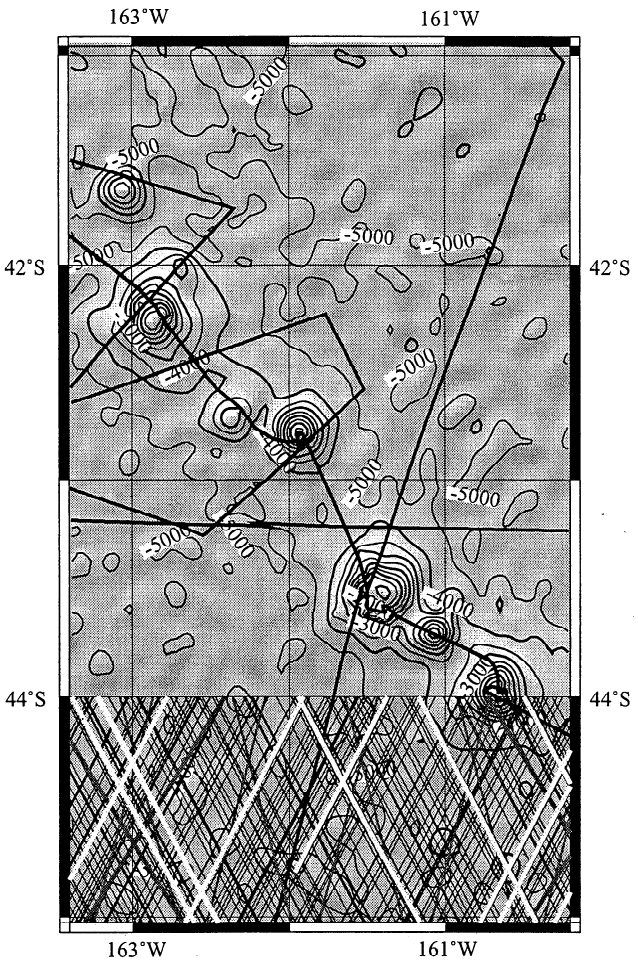

Figure 3. Spatial coverage of satellite data versus ship tracks for region G. Thick black lines represent ship profiles available for the area. Light gray lines are Seasat tracks (used by *Cazenave and Dominh* [1984]). Thin black lines indicate Geosat, TOPEX, and ERS-1 altimeter tracks used in the *Sandwell and Smith* [1997] 2-min gravity grid, version 9.2.

In order to invert the satellite-derived gravity grid to predict bathymetry we first divided the Louisville system into three approximately square regions with sides of length >1000 km (see Plate 1, dashed boxes 1-3) so we could include wavelengths longer than the maximum expected flexural wavelength in our inversion. For each of these large regions we performed the same procedure, iterating over a range of both crustal densities (ρ_c=2600-3000 kg m^{-3}) and elastic thicknesses (T_e=0-50 km). For simplicity, the calculations were performed in the wavenumber domain rather than the spatial domain.

Oldenburg [1974] performed a nonlinear inversion for topography using an iterative method along two-dimensional gravity profiles. We used a different approach: removing an

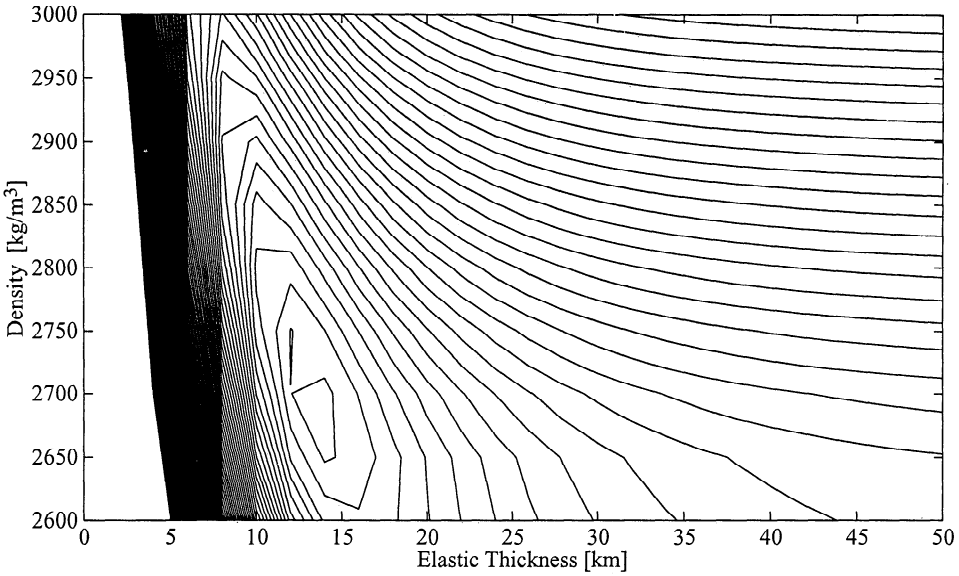

Figure 4. The rms misfit for region G plotted against crustal density, ρ_c, and elastic thickness, T_e, for the nonlinear case. Mantle density is 3400 kg m^{-3}, E=1x10^{11} N m^{-2}, and d=6 km. Minimum rms is 293 m and the contour interval is 5 m. For low elastic thicknesses, variation in ρ_c does not affect the misfit. However, for older, thicker plates a decrease in crustal density translates to an increase in T_e.

estimate of the higher-order gravitational terms ($N(|\mathbf{k}|,t)$ in equation (5)) to yield a solvable linear approximation. This was achieved by estimating the gravitational contribution of terms 2-7 from the predicted bathymetry of *Smith and Sandwell* [1997]. The Smith and Sandwell grid was derived by limiting the waveband to avoid wavelengths where T_e is important and then adjusting the predictions to coincide with the ship bathymetry along surveyed points (for a discussion of this, see *Smith and Sandwell* [1994]). While not exact because of errors in the predicted depths, this should provide a reasonable estimate of the nonlinear contribution as the crests of most seamounts along the chain were surveyed by *Lonsdale* [1988] and included in the *Smith and Sandwell* [1997] bathymetry grid.

This estimate of $N(|\mathbf{k}|,t)$ was then subtracted from the satellite-derived gravity anomaly, yielding an approximate linear equation, $G_{\text{first order}}(\mathbf{k})=Z(|\mathbf{k}|)B(\mathbf{k})$. The admittance function, $Z(|\mathbf{k}|)$, was calculated for each value of ρ_c and T_e and then band-limited, since $1/Z(|\mathbf{k}|)$ suffers from instabilities at both very short wavelengths, owing to low signal-to-noise ratio, and very long wavelengths, owing to downward continuation [*McNutt*, 1979; *Dixon et al.*, 1983; *Baudry and Calmant*, 1991; *Sichoix and Bonneville*, 1996]. Following the example of *Smith and Sandwell* [1994], we constructed a spectral window, $W(\mathbf{k})=W_1(\mathbf{k})*W_2(\mathbf{k})$, where $W_1(\mathbf{k})$ is a high-pass (with wavenumber) cosine filter which ramps between a value of 1 for λ<571 km and 0 for λ>800 km and $W_2(\mathbf{k})$ is a low-pass filter of the form

$$W_2(\mathbf{k})=1/(1+A|\mathbf{k}|^4 e^{4\pi|\mathbf{k}|s}), \quad (6)$$

with A=5x10^{15} m^4 so that the half amplitude occurs at 13, 17, and 20 km for s=2, 4, and 6 km, respectively. This filter preserves data within the "coherent wave band" (25-250 km) [*Ribe and Watts*, 1982; *Ribe*, 1982] in which admittance estimates are of a high reliability (coherence > 0.75). Although $W_1(\mathbf{k})$ places a lower-resolution limit of ~5 km on elastic thickness estimates [*Watts et al.*, 1980; *Smith and Sandwell*, 1994], the expected value for T_e within the Louisville system based on age of the crust at time of loading is 20-25 km, so this should not cause any deleterious effects in our inversion.

After solving for bathymetry for the entire 1000x1000 km^2 region, we inverse Fourier transformed our prediction, $B_{\text{pred}}(\mathbf{k})$, to determine misfits within the spatial domain. We compared $B_{\text{pred}}(\mathbf{x},\mathbf{y})$ within smaller subregions of the 1000x1000 km^2 area (see Plate 1, boxes A-L) to the measured bathymetry along available ship tracks within that subregion. By using this technique of subdividing, we were able to include the long wavelengths necessary in the inversion for bathymetry, but we constrained our solution with precise ship data within smaller regions of interest.

Within each subregion, A-L, we fit our predictions, $B_{\text{pred}}(\mathbf{x},\mathbf{y})$, only at points where ship data were available. These predictions were compared with both the ship bathymetry data ($B_{\text{unf}}(\mathbf{x},\mathbf{y})$, henceforth called "unfiltered"), which was high-pass filtered to remove the mean depth, and a band-pass-filtered version of the ship data ($B_{\text{filt}}(\mathbf{x},\mathbf{y})=F^{-1}\{W_2(\mathbf{k})*B_{\text{unf}}(\mathbf{k})\}$, henceforth called "filtered") which included only the signal within the same waveband as our band-limited admittance function. The rms values for both comparisons within each box were evaluated and plotted to determine the best fitting values for our parameters, ρ_c and T_e.

4. Results and Discussion

Plate 2 shows the magnitude of the gravity anomaly due to terms 2-7 of Parker's equation for subregion G, with a value for ρ_c of 2800 kg m^{-3}. Most of the region yields a nonlinear contribution very close to zero, with a sharp increase in magnitude over the seamounts, peaking to a value of >60 mGal over the summits. This large nonlinear contribution by the short-wavelength features to the total gravity anomaly is not surprising given the results of the model in Figure 2b and demonstrates the importance of these terms in areas with large-amplitude features such as the Louisville chain.

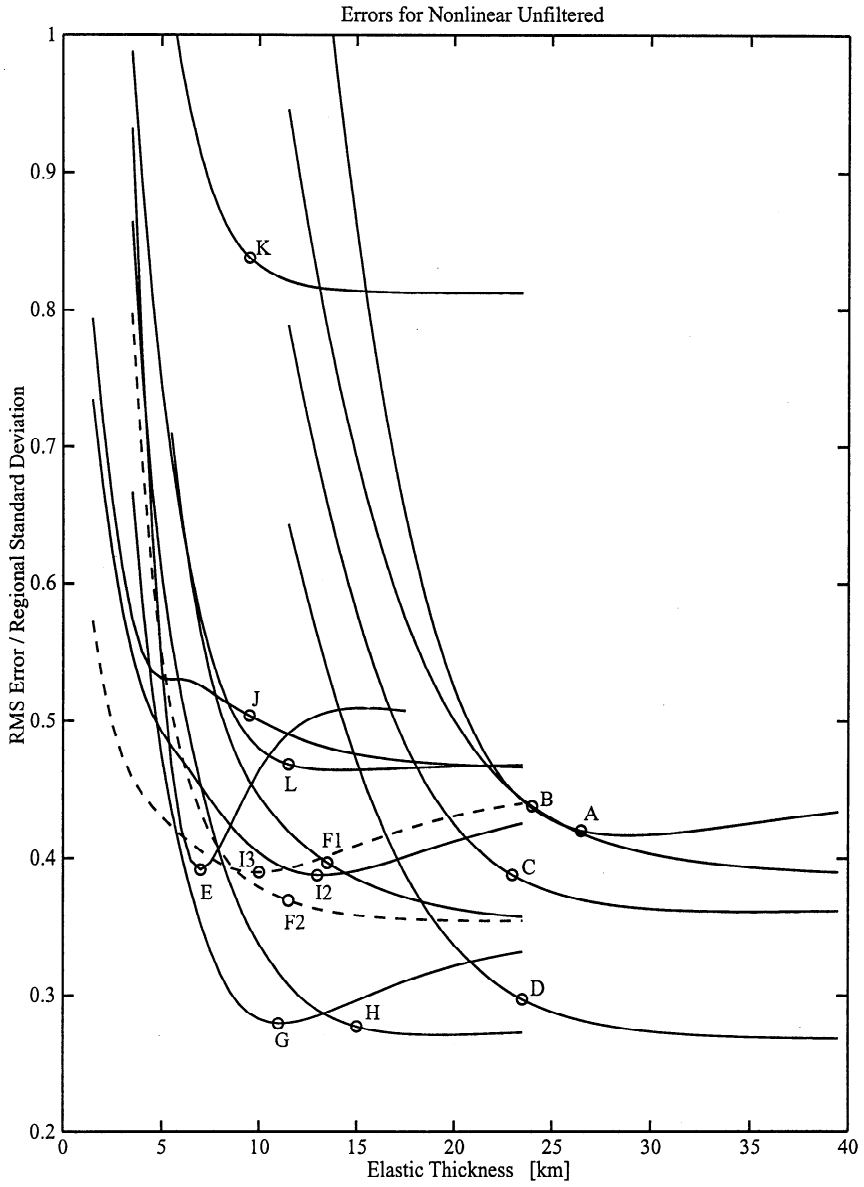

Figure 5. The rms misfit for each region of the Louisville Ridge, using ρ_c=2800 kg m^{-3}, normalized by the standard deviation of the topography within that region. Values are for the nonlinear inversion and show misfit as a percentage of the variation of topography. The circles represent the best fit value of the elastic thickness and are at the point of maximum curvature. For region J the point of maximum curvature for T_e>6 km was used owing to the anomalous kink in the misfit curve at T_e=5 km (the resolution limit of this method). These values are listed in Table 1 along with the lower and (where possible) upper bounds. Bounds are at ±5% misfit from the best-fit value. While the lower bound on T_e can be determined for all regions, the upper bound is complicated by the pseudo-asymptotic behavior as T_e grows large. This is due to the negligible change in deflection caused by an emplaced load once the elastic thickness reaches a critical value.

To determine the effect of various parameters on elastic thickness estimates, we varied crustal density in our inversion between 2600 and 3000 kg m^{-3}. An example of rms misfit for varying ρ_c and T_e within region G is shown in Figure 4. As can be seen in this plot, for areas with low elastic thickness, variation in ρ_c has little effect on misfit. However, for older, thicker plates, a reduction in crustal density forces an increase in the elastic thickness estimate. If it is assumed that the crustal density remains constant along the chain, then a density that is too high or too low will affect the magnitude of T_e, but the trend of values along the chain will remain the same. Variation in the value for Young's modulus yields a similar result. We used E=1x10^{11} N m^{-2} for our calculations, but a smaller value, such as E=6.5x10^{10} N m^{-2} [*Sandwell*, 1984], increased the T_e for each region by ~6%. Again, by assuming that E is constant along the chain, only the magnitude of T_e is affected, and the tectonic implications of the estimates should remain the same.

Thus it should be noted that the trend of elastic thickness estimates along a seamount chain is generally more informative than the magnitude, owing to the effects of variation in initial parameters on T_e estimates [e.g., *Calmant et al.*, 1990; *Burov and Diament*, 1995, *Sichoix and Bonneville*, 1996].

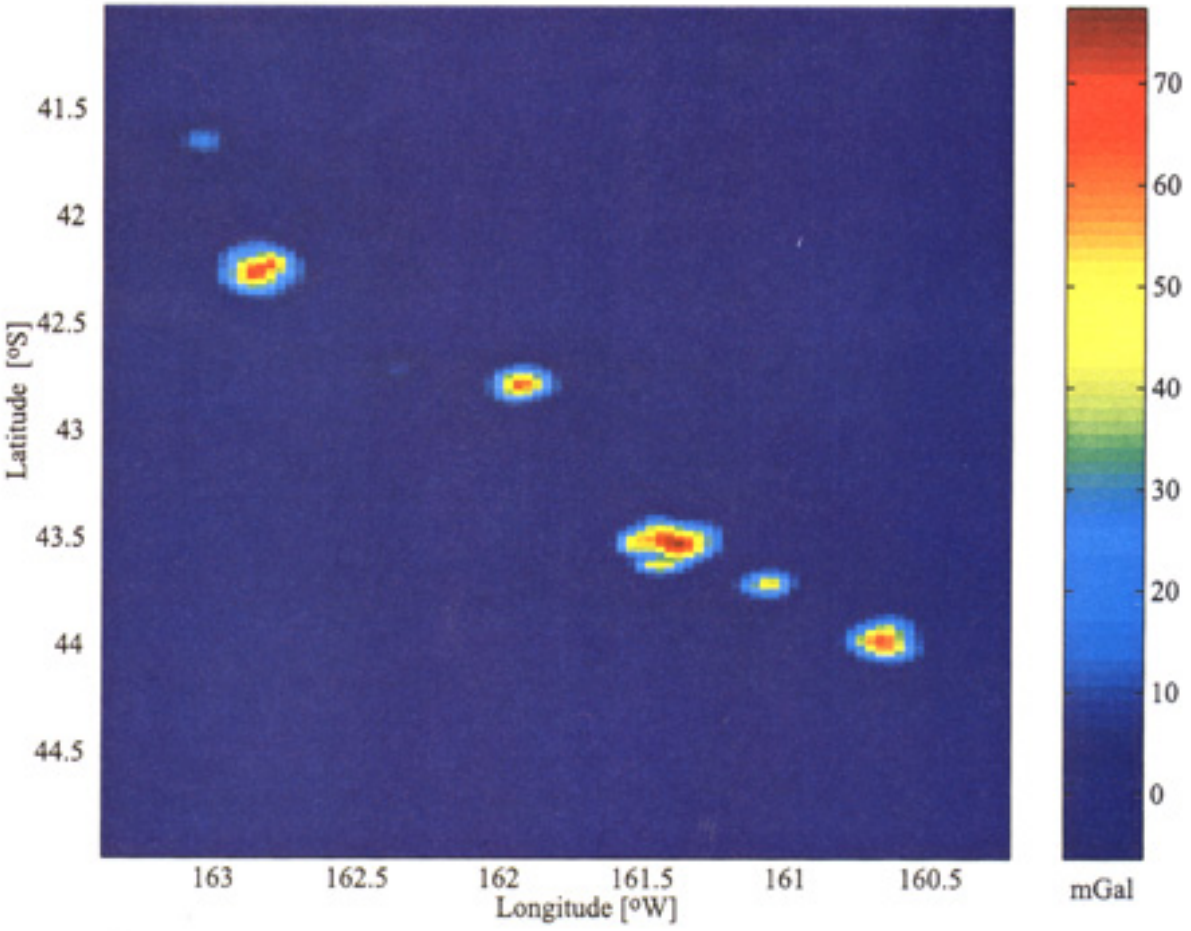

Plate 2. Nonlinear contribution of topography to the gravitational anomaly. $G(\mathbf{k})$ for n=2-7 from *Parker's* [1973] equation is shown for region G of the Louisville Ridge. Most of the region has a negligible nonlinear effect, but over the larger features, gravitational contribution from the higher-order terms grows quite large.

Table 1. Best Fitting Elastic Thickness Values From *Watts et al.* [1988], *Cazenave and Dominh* [1984], and This Study

Profile	Expected	Watts	Cazenave 2-D	Cazenave 3-D	Nonlinear			Linear			Region
					Lower	Best	Upper	Lower	Best	Upper	
1	(22)	12.5 - 17.5		21.7 - 23.1	22	26.5		23	27		A
2	(22)	10.0 - 20.0	15.0 - 20.0	18.6 - 21.4	21	24		21.5	24		B
3	(22)	10.0 - 17.0			19.5	24		21.5	24		B
4	(22)	<15.0		12.8 - 18.8	19.5	23		20	23		C
5	(22)	12.5 - 20.0			19.5	23		20	23		C
6	(22)	30.0 - 37.5			19.5	23.5		19.5	23		D
7	(22)				19.5	23.5		19.5	23		D
8	22	34.0 - 41.0	12.0 - 15.0	16.6 - 19.0	6	7	9	6.5	8	12	E
9	22.5				10	13.5		12	15.5		F1
10	22.5	27.5 - 32.5	10.0 - 12.0	16.6 - 17.8	10	13.5		12	15.5		F1
9	22.5				7.5	11.5		9	13		F2
10	22.5	27.5 - 32.5	10.0 - 12.0	16.6 - 17.8	7.5	11.5		9	13		F2
11	23	37.5 - 42.5	12.0 - 15.0	16.6 - 19.0	8	11	22.5	9.5	14		G
12	23	32.5 - 42.5	12.0 - 15.0	16.6 - 19.0	8	11	22.5	9.5	14		G
	23				10.5	15		12	15.5		H
	23				8	13	28	11	14.5		I2
	23				4.5	10	23	8.5	12		I3
	22.5				4	9.5		6.5	10		J
	22				8	9.5		9	9.5		K
	22				8.5	11.5		10	12		L

Ship profile, as used by *Watts et al.* [1988], the regions in this study, including not only the corresponding profiles from the previous studies, but all other ship data available within that area since our technique is not constrained by the requirement of profile alignment perpendicular to the feature. Nonlinear represent bound estimates using the nonlinear approximation for the topographic contribution to gravity, while the Linear represent bounds from the linear approximation as discussed in the text. Best estimate is the point of maximum curvature in Figure 5 for each region. The lower and upper bounds represent ±5% of the normalized misfit. While our results are in agreement with the general trend of *Cazenave and Dominh*'s [1984] 3-D estimate, we find a distinctive jump in elastic thickness at region E. Our results are in general disagreement with values from *Watts et al.* [1988], presumably due to both improved data sets and the inclusion of proper dimensionality.

The best fitting T_e values within each region are provided in Table 1, compared with the previous results of *Watts et al.* [1988] and *Cazenave and Dominh* [1984]. Even though our best fit values for crustal density varied somewhat for the regions, we evaluated misfit for ρ_c=2800 kg m^{-3} for consistency of comparison with the previous studies.

Cazenave and Dominh [1984] used analog bathymetric maps from *Mammericx et al.* [1974] to model geoid height in three dimensions, which they compared to geoid values derived from Seasat altimeter data. They also performed 2-D spectral analyses along profiles of ship data for comparison. It is interesting to note that their 3-D estimates yield a T_e that is typically ~4 km higher than their 2-D values. In their discussion, Cazenave and Dominh attribute this to the dimensionality issue, positing that a two-dimensional assumption leads to an overestimate of lithospheric deflection (shown by *Watts et al.* [1975] and confirmed in Figure 2c) and a corresponding negative geoid anomaly. This, they claim, added to an overestimate of the positive geoid anomaly caused by topography (which we do not see in Figure 2c) yields an overestimate of the total anomaly and a smaller derived plate thickness as compared to the 3-D approach.

However, as can be determined from Figure 2, and discussed by *Ribe* [1982] and *Watts et al.* [1988], a feature which is inherently two-dimensional prefers a higher elastic thickness than that of a more circular, three-dimensional feature. Therefore, the improper assumption of dimensionality for a seamount would actually result in an overestimate of elastic thickness. Thus, the contradictory nature of *Cazenave and Dominh's* [1984] results is probably due to the poor quality of the data sets and the insufficient coverage of the earlier altimeter data.

Watts et al. [1988] estimated elastic thicknesses for the Louisville chain using two-dimensional ship data, including that obtained during the 1984 survey by the R/V *Thomas Washington*. While the magnitude of their estimates in the northwestern region of the chain appears to agree somewhat with *Cazenave and Dominh's* [1984] results, Watts et al. find much higher best fitting values in the southeast, and the general trend (increasing T_e from northwest to southeast) is the opposite, which they partially attribute to dimensionality differences.

Our results tend to agree with *Cazenave and Dominh* [1984] in trend and show increasing values from southeast to northwest. The rms misfit for the nonlinear inversion (unfiltered comparison) for all regions is shown in Figure 5. The rms is normalized by the standard deviation of the region and represents the ratio of error in our estimate to the variation in topography. Circles represent the best fit estimate of elastic thickness and are the point of maximum curvature of the misfit. This plot illustrates not only the bimodal nature of the elastic thicknesses under the two sections of the chain (A-D and F-L) but also shows the difficulty in assessing an upper bound on the T_e estimates. In most cases, the misfit does not significantly increase as T_e grows large, owing to the negligible change in deflection (and, hence, gravitational anomaly) caused by an emplaced bathymetric load once the elastic thickness has passed a critical value.

Table 1 shows the estimates and bounds (where possible) for elastic thickness values for both the nonlinear and linear cases within each region. Bounds were determined by ±5% of the normalized misfit for the best T_e value. This leads to a lower bound in all cases but an upper bound in only a few regions. In general, the pattern of best T_e estimates for all four cases is the

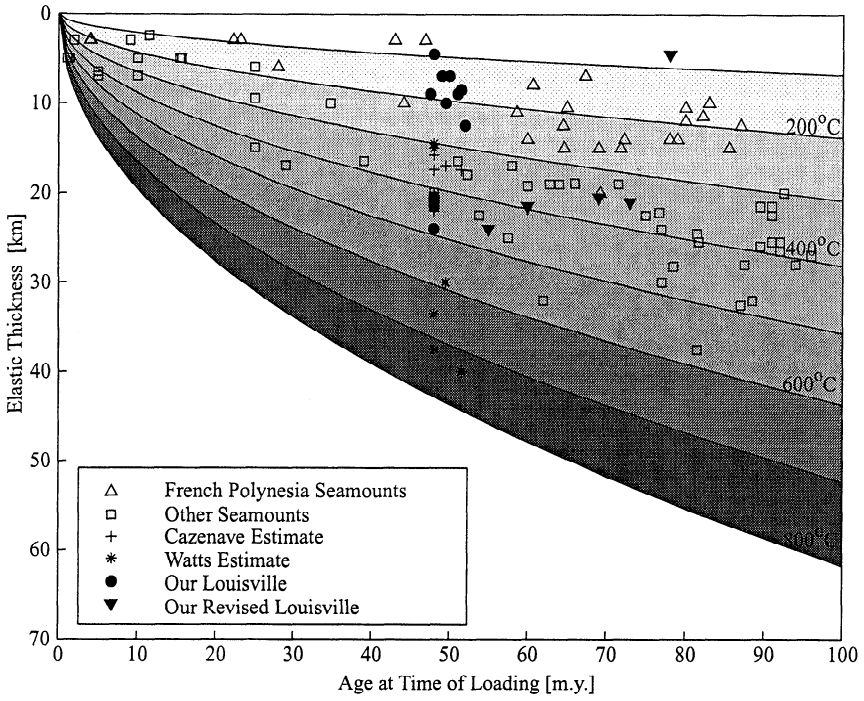

Figure 6. Elastic thickness versus age at time of loading. Data are taken from Figure 1 of *Wessel* [1992] and illustrates the relationship first proposed by *Watts* [1978], which states that the elastic thickness under seamounts follows the 450°±150°C isotherm based on the cooling plate model of *Parsons and Sclater* [1977]. Although seamounts within French Polynesia (triangles) yield lower-than-expected values, estimates of T_e from other regions of the world's oceans (squares) fall within these bounds. Solid circles represent our results for the Louisville Ridge. Age at time of loading for Louisville is based on crustal ages taken from *Mueller et al.* [1997] and seamount ages from *Lonsdale* [1988]. North of region E, where data are not available from *Mueller et al.* [1997], age is assumed to increase linearly with distance along the chain. Solid triangles represent our estimates using revised ages approximated from the tentative tectonic history of *Lonsdale* [1997] which places an age discontinuity at ~39°S along the ridge.

same: a relatively low value (~11 km) in the southeast, increasing slightly toward the northwest, with a sharp anomaly (7 km) in region E, followed by a higher value (~24 km) northwest of E which increases toward the northwest.

Watts [1978] showed that the elastic thickness for the Hawaiian chain agreed with the depth to the 450° ± 150°C isotherm based on the cooling model of *Parsons and Sclater* [1977]. This result has been supported by numerous studies since [e.g., *Watts and Ribe*, 1984; *Calmant et al.*, 1990]. Figure 6, based on the data in Figure 1 of *Wessel* [1992], shows that, for most seamounts outside of French Polynesia, the elastic thickness does indeed fall between the 300° and 600°C isotherms. The solid circles in Figure 6 indicate our estimates for the Louisville region, with crustal ages taken from *Mueller et al.* [1997] and seamount ages from *Lonsdale* [1988]. Along the northwest section (A-D), where age data are not available, we estimated crustal ages based on the assumption of linear age progression with distance along the ridge.

Our elastic thickness estimates for Louisville are lower than expected in the southeastern region (F-L) and are similar to those obtained in French Polynesia. This low T_e could be due to the presence of the nearby Eltanin Fracture Zone system, which formed prior to the emplacement of the Louisville Ridge [*Watts et al.*, 1988]. However, since the southeastern region of the chain is composed of numerous isolated, circular features, and most of the studies included in Figure 6 were performed assuming two-dimensional features, the lower than expected elastic thicknesses from our study could also reflect the effect of considering correct dimensionality for these seamounts. T_e values in the northwest section (A-D) of the Louisville system, when compared to the southern section, are higher than expected, implying that the northern seamounts formed on an older plate than the southern ones and that our assumption of continuous age progression of the plate is not correct. There is an anomaly in the elastic thickness estimates (T_e=7 km) at 39°S, dividing the northern region from the southern.

The location of this T_e jump is coincident with an anomaly in the gravity field: the signature of the Wishbone scarp (see Plate 1). This scarp is thought to be a remnant transform fault which had formed from the extinct spreading ridge located at ~25°S, halfway between the Manihiki and Hikurangi plateaus [*Lonsdale*, 1997]. According to P. Lonsdale (personal communication, 1999), this remnant boundary could account for a crustal age discontinuity of anywhere from 5 to 25 Ma, which would explain the increased elastic thickness estimates to the northwest of the scarp. Shown in Figure 6 (solid triangles) are the revised T_e versus age values for the northwestern region based on this tentative new model, which increases the age at the time of loading by 7 Ma on the northwest side of the scarp and by up to 30 Ma at the Osbourn Trough. These new T_e estimates fall very close to the 400°C isotherm. The 1999 AVON04 cruise by the R/V *Melville* to this region will place better constraints on the crustal age and assist in untangling the complex tectonic history of this area.

Figure 7 shows the predicted topography along profile 12 over a seamount in region G (43.5°S, 161.5°W) using our elastic thickness estimate (11 km, short-dashed), *Cazenave and Dominh's* [1984] 3-D result (17.8 km, dotted), and *Watts et al.'s* [1988]

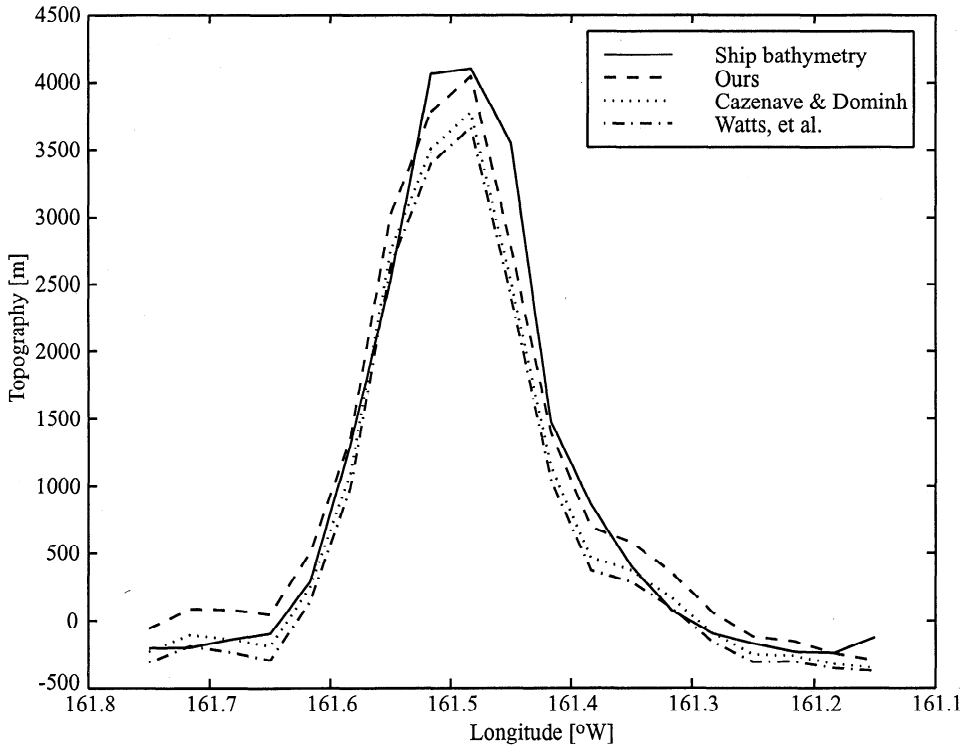

Figure 7. Comparison of topographic prediction with ship bathymetry for profile 12 over the seamount in region G. Predicted bathymetry is shown for a range of elastic thickness values: our estimate (11 km, short-dashed), *Cazenave and Dominh's* [1984] (17.8 km, dotted), and *Watts et al.* [1988] (37.5 km, dash-dotted). The actual ship bathymetry (high-pass filtered to remove the mean) is shown as a solid line. The rms misfits between predicted and actual ship bathymetry for this profile are 267.43 m, 334.91 m, and 393.82 m for our study, *Cazenave and Dominh's* [1984], and *Watts et al.* [1988], respectively.

value (37.5 km, dash-dotted) compared with the actual ship bathymetry (solid). Our estimate has the lowest rms misfit when compared to the actual ship bathymetry (267.43 m), followed by Cazenave and Dominh (334.91 m) and Watts et al. (393.82 m). Comparison with the band-passed bathymetry yields a much better fit in each case (201.17 m, 299.03 m, and 368.57 m, respectively). While all three methods model the sides of the seamount with similar accuracy, the higher T_e values do not predict the peak of the seamount as well as our value of 11 km.

Inclusion of the nonlinear terms in our inversion did not have a large effect on the elastic thickness estimates, with T_e values from the linear method exceeding those from the nonlinear by a mean

Table 2. Minimum rms Misfit Value Within Each Region

Region	Regional STD		Unfiltered	Filtered	Linear Unfiltered	Linear Filtered	Difference, %*	
	Unfiltered	Filtered					Unfiltered	Filtered
A	1009	952	418	377	421	413	1	9
B	948	889	354	306	352	325	-1	6
C	953	888	339	254	331	279	-2	9
D	1120	1093	299	230	342	299	13	23
E	1523	1508	560	544	566	557	1	2
F1	1188	1158	418	371	425	390	2	5
F2	1188	1144	418	368	455	432	8	15
G	1075	1026	293	208	301	275	3	24
H	1067	1037	288	209	337	294	15	30
I2	779	716	275	217	251	210	-10	-3
I3	779	687	275	209	248	216	-11	3
J	600	527	274	182	257	188	-7	3
K	247	107	196	128	194	127	-1	-1
L	654	569	301	163	272	151	-11	-8

Values represent the minimum misfit for the region for each of the four inversion cases. Percent difference illustrates the decrease in misfit attained by including the nonlinear terms. Misfit is reduced by up to 30% by including the higher-order effect in areas with large variance in topography, but misfit increases by up to 10% in areas where the variance is small.

*Percent decrease in minimum rms by including nonlinear terms [(linear-nonlinear)/linear *100].

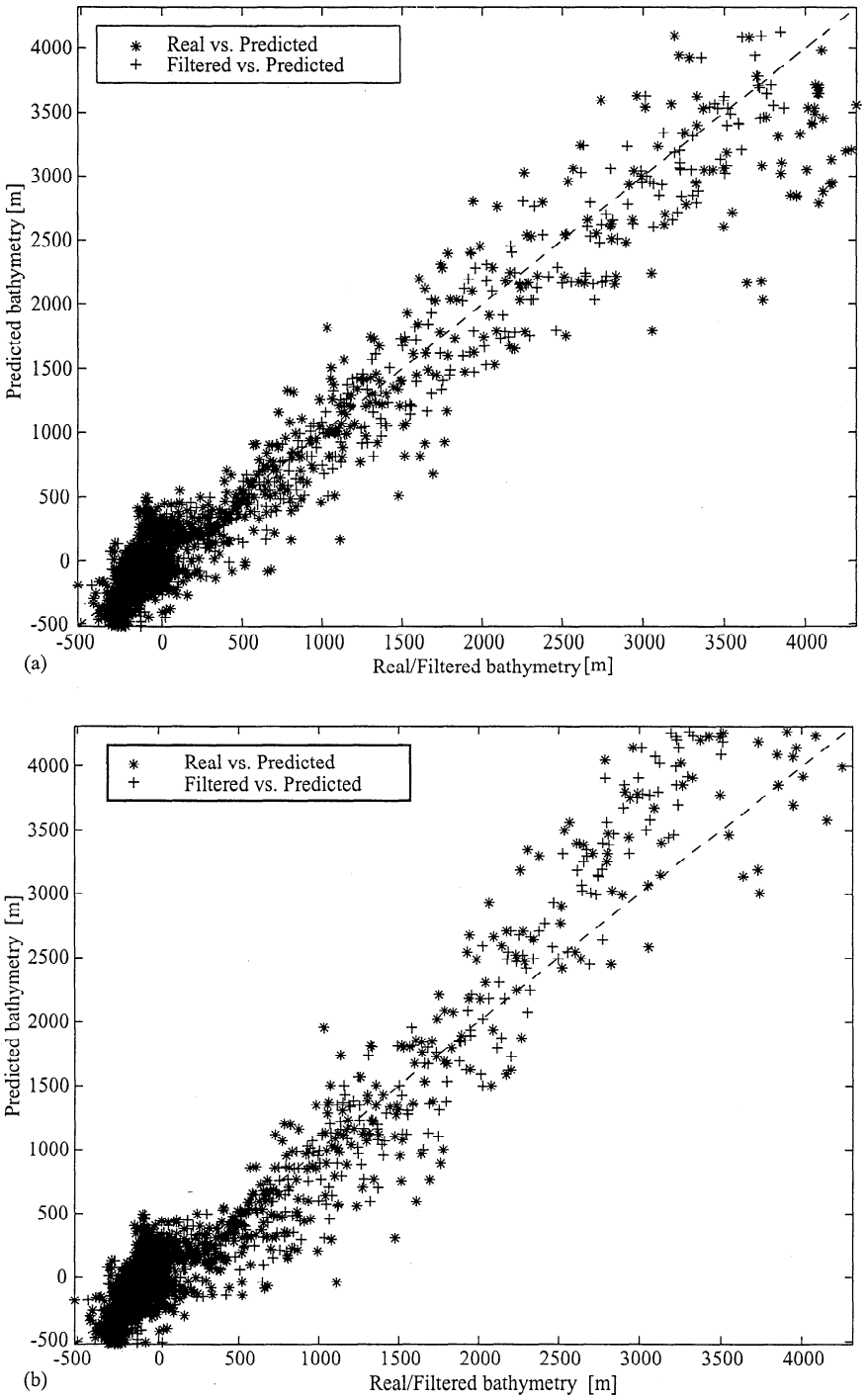

Figure 8. Real versus predicted bathymetry for region G. Predicted bathymetric values (calculated with T_e=11 km and ρ_c=2800 kg m^{-3}) for each point along tracks in the grid (993 points) are plotted versus their respective ship value. All ship data have been high-pass-filtered to remove the mean value of the region. The dashed line indicates the 1:1 exact fit value. Stars represent high-pass-filtered ship bathymetry. Crosses represent ship values that have also been bandlimited as discussed in the text. For both the (a) nonlinear and (b) linear inversions the band-limited comparison confines the points closer to the 1:1 line. However, for large features the linear inversion overpredicts the bathymetry, signifying a T_e value that is too low. The best fit value for the linear case in this region is 14 km.

of 0.86 km (median of 0.50 km) for unfiltered bathymetry and a mean of 0.61 km (median of 0.50 km) for filtered bathymetry. The largest discrepancies between the linear and nonlinear estimates (2-3 km) occurred in the middle to southern end of the chain where there are isolated, short-wavelength seamounts on younger, thinner crust than in the northwest.

Figures 8a and 8b show the correlation between the real bathymetry and the predicted bathymetry for region G, which contains circular, short-wavelength features. In Figure 8a, the nonlinear estimate, predictions are well correlated with both the unfiltered bathymetry (stars) as well as with the band-passed bathymetry (crosses), with the latter case showing an improved

match over the former. The same holds true in general for the linear method (Figure 8b), but we see that for large features on the seafloor (> 2 km) the predicted bathymetry is too high, signifying an elastic thickness value which is too low. Thus the linear method within this region yields a best fitting T_e which is ~3 km greater than that by the nonlinear method.

As mentioned previously, the correlation improves for the comparison with band-pass-filtered topography, but the actual effect of filtering on the elastic thickness estimate is quite small, with the filtered T_e greater than the unfiltered value by a mean of 0.61 km (median of 0.50 km) for the nonlinear case and a mean of 0.32 km (median of 0.25 km) for the linear case. This difference is not dependent on location along the chain.

5. Conclusions

Including the nonlinear terms in our inversion improved our elastic thickness fit, reducing the minimum rms misfit by 1-30% in areas with a large standard deviation of topography (see Table 2). In the southeast region, however, where the variance in depth for the region is not as great, the linear estimate actually had a somewhat lower minimum rms misfit than the nonlinear when the predictions were compared to the unfiltered bathymetry. The resultant effect of including the nonlinear terms in the estimation of elastic thickness was small, with ~1-2 km greater value for the linear estimates than for the nonlinear determinations.

In contrast, the dimensionality of the features in question appears to have a large effect on elastic thickness determination in flexure studies. Since there is a higher percentage of depth soundings over the broad flanks than the narrow peaks, the dimensionality issue was emphasized and could assist in explaining some of the disparity between our study and previous, two-dimensional ones [*Cazenave and Dominh*, 1984; *Watts et al.*, 1988]. It also provides a viable reason for the low values of elastic thickness in Figure 6, when compared with the T_e versus age relationship of other Pacific seamounts.

This approach is particularly effective for estimation of elastic thickness in regions where ship tracks do not cross seamount peaks or where data are sparse. However, our elastic thickness estimates should be considered lower bounds rather than absolute values, as the upper limits can be very difficult to define due to the asymptotic behavior of the misfit for large T_e (see Figure 5). Therefore the best constraint for a reasonable upper bound would usually be found using the age of the crust at the time of loading

Acknowledgments. The authors would like to thank Peter Lonsdale for providing information on the crustal ages and spreading history of the Louisville region. We also thank R. L. Parker for his questions and constructive comments on the first draft of this manuscript. Many of the figures were created using the GMT software of *Wessel and Smith* [1991]. Reviews and suggestions by M. Diament, C. Ebinger, and P. Wessel led to a considerably improved final version of this paper. This work was supported by a Department of Defense, National Defense Science and Engineering Graduate Fellowship (S.N. Lyons), National Science Foundation grant OCE-9521518, and NASA grant NAG5-5176.

References

Banks, R.J., R.L. Parker, and S.P. Huestis, Isostatic compensation on a continental scale: Local versus regional mechanisms, *Geophys. J. R. Astron. Soc., 51,* 431-452, 1977.

Baudry, N., and S. Calmant, 3-D modelling of seamount topography from satellite altimetry, *Geophys. Res. Lett., 18,*1143-1146, 1991.

Burov, E.B., and M. Diament, The effective elastic thickness (T_e) of continental lithosphere: what does it really mean?, *J. Geophys. Res., 100*, 3905-3927, 1995.

Calmant, S., J. Francheteau, and A. Cazenave, Elastic layer thickening with age of the oceanic lithosphere: A tool for prediction of the age of volcanoes or oceanic crust, *Geophys. J. Int., 100,* 59-67, 1990.

Cazenave, A., and K. Dominh, Geoid heights over the Louisville Ridge (South Pacific), *J. Geophys. Res., 89*, 11,171-11,179, 1984.

Dixon, T.H., M. Naraghi, M.K. McNutt, and S.M. Smith, Bathymetric prediction from Seasat altimeter data, *J. Geophys. Res., 88*, 1563-1571, 1983.

Dorman, L.M., and B.T.R. Lewis, Experimental isostasy, 1, Theory of the determination of the Earth's isostatic response to a concentrated load, *J. Geophys. Res., 75*, 3357-3365, 1970.

Goodwillie, A.M., Short-wavelength gravity lineations and unusual flexure results at the Puka Puka volcanic ridge system, *Earth Planet. Sci. Lett., 136*, 297-314, 1995.

Hébert, H., B. Villemant, C. Deplus, and M. Diament, Contrasting geophysical and geochemical signatures of a volcano at the axis of the Wharton fossil ridge (N-E Indian Ocean), *Geophys. Res. Lett., 26*, 1053-1056, 1999.

Kogan, M.G., M. Diament, A. Bulot, and G. Balmino, Thermal isostasy in the South Atlantic Ocean from geoid anomalies, *Earth Planet. Sci. Lett., 74*, 280-290, 1985.

Lewis, B.T.R., and L.M. Dorman, Experimental isostasy, 2, An isostatic model for the United States derived from gravity and topographic data, *J. Geophys. Res., 75*, 3367-3386, 1970.

Lonsdale, P., A multibeam reconnaissance of the Tonga Trench axis and its intersection with the Louisville Guyot Chain, *Mar. Geophys. Res., 8,* 295-327, 1986.

Lonsdale, P., Geography and history of the Louisville hotspot chain in the southwest Pacific, *J. Geophys. Res., 93*, 3078-3104, 1988.

Lonsdale, P., An incomplete geologic history of the southwest Pacific basin, *Geol. Soc. Am. Abstr. Programs, 29 (5)*, 25, 1997.

Mammericx, J., S.M. Smith, I.L. Taylor, and T.E. Chase, Bathymetry of the South Pacific, *I M R TR-45 Sea Grant Publ. 12*, Scripps Inst. of Oceanogr., La Jolla, Calif., 1974.

McConathy, D.R., and C.C. Kilgus, The Navy Geosat mission: An overview, *Johns Hopkins APL Tech. Dig., 8*, 170-175, 1987.

McKenzie, D., and C. Bowin, The relationship between bathymetry and gravity in the Atlantic Ocean, *J. Geophys. Res., 81*, 1903-1915, 1976.

McNutt, M.K., Compensation of oceanic topography: an application of the response function technique to the Surveyor area, *J. Geophys. Res., 84*, 7589-7598, 1979.

McNutt, M.K., and R.L. Parker, Isostasy in Australia and the evolution of the compensation mechanism, *Science, 199*, 773-775, 1978.

Moore, J.G., Relationship between subsidence and volcanic load, Hawaii, *Bull. Volcanol., 34,* 562-576, 1970.

Mueller, R.D., W.R. Roest, J.-Y. Royer, L.M. Gahagan, and J.G. Sclater, Digital isochrons of the world's ocean floor, *J. Geophys. Res., 102*, 3211-3214, 1997.

Oldenburg, D.W., The inversion and interpretation of gravity anomalies, *Geophysics, 39*, 526-536, 1974.

Parker, R.L., The rapid calculation of potential anomalies, *Geophys. J. R. Astron. Soc., 31*, 447-455, 1973.

Parsons, B., and J.G. Sclater, An analysis of the variation of ocean floor bathymetry and heat flow with age, *J. Geophys. Res., 82*, 803-827, 1977.

Ribe, N.M., On the interpretation of frequency response functions for oceanic gravity and bathymetry, *Geophys. J. R. Astron. Soc., 70*, 273-294, 1982.

Ribe, N.M. and A.B. Watts, The distribution of intraplate volcanism in the Pacific Ocean basin: A spectral approach, *Geophys. J. R. Astron. Soc., 71*, 333-362, 1982.

Sandwell, D.T., Thermomechanical evolution of oceanic fracture zones, *J. Geophys. Res., 89*, 11,401-11,413, 1984.

Sandwell, D.T., and W.H.F. Smith, Marine gravity anomaly from Geosat and ERS-1 satellite altimetry, *J. Geophys. Res., 102*, 10,039-10,054, 1997.

Sandwell, D. T., E.L. Winterer, J. Mammericx, R.A. Duncan, M.A. Lynch, D. Levitt, and C. Johnson, Evidence for diffuse extension of the Pacific Plate from Pukapuka Ridges and cross-grain gravity lineations, *J. Geophys. Res., 100*, 15,087-15099, 1995.

Sichoix, L., and A. Bonneville, Prediction of bathymetry in French Polynesia constrained by shipboard data, *Geophys. Res. Lett., 23*, 2469-2472, 1996.

Smith, W.H.F., and D.T. Sandwell, Bathymetric prediction from dense satellite altimetry and sparse ship bathymetry, *J. Geophys. Res., 99*, 21,803-21,824, 1994.

Smith, W.H.F., and D.T. Sandwell, Global seafloor topography from satellite altimetry and ship depth soundings, *Science, 277*, 1956-1962, 1997.

Suyenaga, W., Isostasy and flexure of the lithosphere under the Hawaiian Islands, *J. Geophys. Res., 84*, 5599-5604, 1979.

Vening Meinesz, F.A., Gravity over the Hawaiian Archipelago and over the Madeira area: Conclusions about the Earth's crust, *Proc. K. Ned. Akad. Wet., 44,* 1, 1941.

Walcott, R.I., Flexure of the lithosphere at Hawaii, *Tectonophysics, 9*,435-446, 1970.

Watts, A.B., An analysis of isostasy in the world's oceans, 1, Hawaiian-Emperor seamount chain, *J. Geophys. Res., 83*, 5989-6004, 1978.

Watts, A.B., On geoid heights derived from Geos 3 altimeter data and flexure along the Hawaiian-Emperor seamount chain, *J. Geophys. Res., 84*, 3817-3826, 1979.

Watts, A.B., and J.R. Cochran, Gravity anomalies and flexure of the lithosphere along the Hawaiian-Emperor Seamount Chain, *Geophys. J. R. Astron. Soc., 39,* 119-141, 1974.

Watts, A.B., and N.M. Ribe, On geoid heights and flexure of the lithosphere at seamounts, *J. Geophys. Res., 89*, 11,152-11,170, 1984.

Watts, A.B., and U.S. ten Brink, Crustal structure, flexure, and subsidence history of the Hawaiian islands, *J. Geophys. Res., 94,* 10,473-10,500, 1989.

Watts, A.B., J.R. Cochran, and G. Selzer, Gravity anomalies and flexure of the lithosphere: A three-dimensional study of the Great Meteor seamount, northeast Atlantic, *J. Geophys. Res., 80*, 1391-1398, 1975.

Watts, A.B., J.H. Bodine, and N.M. Ribe, Observations of flexure and the geological evolution of the Pacific Ocean basin, *Nature, 283,* 532-537, 1980.

Watts, A.B., J.K. Weissel, R.A. Duncan, and R.L. Larson, Origin of the Louisville Ridge and its relationship to the Eltanin Fracture Zone system, *J. Geophys. Res., 93*, 3051-3077, 1988.

Wessel, P., Thermal stresses and the bimodal distribution of elastic thickness estimates of the oceanic lithosphere, *J. Geophys. Res., 97*, 14,177-14,193, 1992.

Wessel, P., A reexamination of the flexural deformation beneath the Hawaiian Islands, *J. Geophys. Res., 98*, 12,177-12,190, 1993.

Wessel, P., and W.H.F. Smith, Free software helps map and display data, *Eos Trans. AGU, 72*, 441, 445-446, 1991.

S. N. Lyons and D. T. Sandwell, Scripps Institution of Oceanography, UCSD, MC0225, La Jolla, CA 92093-0225. (slyons@radar.ucsd.edu, sandwell@geosat.ucsd.edu)

W. H. F. Smith, NOAA Laboratory for Satellite Altimetry, E/OC2, SSMC3, Room 3620, Silver Spring, MD 20910-3282. (wsmith@nodc.noaa.gov)

(Received August 12, 1999; revised January 21, 2000;
accepted February 24, 2000.)